Original

Gan, W.; Hofmann, M.; Ventzke, V.; Randau, C.; Huang, Y.; Kriele, A.; Brokmeier, H.-G.; Müller, M.:

Microstructure and Residual Stress in Rotary Friction Welded Dissimilar Metals of AA7020 Aluminium Alloy with 316L Steel.

In: Sommitsch C.; Ionescu M.; Mishra B.; Mishra B.; Kozeschnik E.; Chandra T. (eds.): Materials Science Forum. Vol. 879 Zürich-Stafa: Trans Tech Publications, 2017. 572 - 577.

First published online by Trans Tech Publications: November 2016

https://dx.doi.org/10.4028/www.scientific.net/MSF.879.572

Materials Science Forum *Online: 2016-11-15*
ISSN: 1662-9752, Vol. 879, pp 572-577
doi:10.4028/www.scientific.net/MSF.879.572
© 2017 Trans Tech Publications Ltd, Switzerland

Microstructure and Residual Stress in Rotary Friction Welded Dissimilar Metals of AA7020 Aluminium Alloy with 316L Steel

Weimin Gan[1*], Michael Hofmann[2], Volker Ventzke[1], Christian Randau[3], Yuanding Huang[1], Armin Kriele[1], Heinz-Guenter Brokmeier[1] and Martin Mueller[1]

[1]Institute of Materials Research, Helmholtz-Centre Geesthacht, D-21502, Geesthacht, Germany

[2] Heinz Maier-Leibnitz Zentrum (MLZ), Technische Universität München, D-85748 Garching, Germany

[3]Institute of Materials Science and Engineering, Clausthal University of Technology, D-38678 Clausthal-Zellerfeld, Germany

Keywords: friction welding, dissimilar metals, residual stress, texture

Abstract. Rotary friction welding (RFW) was used in the current study to join the dissimilar metals AA7020-T6 aluminium alloy and 316L steel. Neutron diffraction was performed to investigate the texture gradient around the weld line and to map the residual stress over the whole specimen. The texture analysis showed a weak shear component near the bond line of AA7020-T6 -T6 side which indicated a plastic deformation of AA7020-T6 during welding. The shear bands were also observed in optical microstructures. Relatively high tensile residual stresses were observed near the bond line on the AA7020-T6 side, which were in-homogeneously distributed from the perimeter to the rod centre, while high compressive residual stresses were found in the sample centre at the bond line in the 316L steel.

Introduction

Rotary friction welding (RFW) is a joining technique for metals in which the welding temperature stays below the melting point and was the first of the friction processes to be developed and used commercially [1]. No additional filler material is used and welding takes place in the solid phase during RFW, i.e. no macroscopic melting is observed. Since there is nearly no limitation to weld any metals the use of RFW for joining dissimilar materials has considerably been increased over the years, mainly in the aerospace industry. Here conventional structures made of steel have been replaced by lightweight materials, such as Al, Ti, and even Mg alloys [2-7]. Especially joining aluminium alloys to stainless steel or carbon steel via RFW has been widely investigated, as in conventional fusion welding formation of brittle intermetallic phases limit the bonding strength between the dissimilar metals [2]. By optimizing RFW welding parameters and the geometry of components the bond strength of Al to cast iron could be increased [4]. In addition the effects of carbon content on the steel side on the quality of such welds were also studied [3].

Other difficult to weld metals like high strength to weight ratio Ti alloys have also been investigated with the aim to obtain good performance welded specimen using RFW [5]. For instance in dissimilar weld TiAl-Ti6Al4V joints the microstructure and micro texture development as a function of friction welding parameters was studied [6]. Preliminary work on the RFW of a Fe_3Al based oxide dispersion strengthened alloy was performed in both recrystallized and non-recrystallized conditions [7].

Plastic deformation can occur during joining especially in dissimilar materials which have large differences in yield strength [8]. In addition due to different thermal expansion coefficients of both metals in a dissimilar weld large residual stresses develop in RFW process, which might influence the properties in real service.

In the present work, AA7020-T6 and 316L steel were successfully joined by RFW process. The interfacial microstructure of the dissimilar weld with particular emphasis on local properties as

All rights reserved. No part of contents of this paper may be reproduced or transmitted in any form or by any means without the written permission of Trans Tech Publications Ltd, www.scientific.net. (#580888892, Helmholtz-Zentrum hereon GmbH, Geesthacht, Germany-28/01/22,12:42:13)

micro hardness, chemical composition and stress distribution has been studied. Moreover, preferred orientation (texture) analysis around the welding zone was performed to elucidate possible deformation or temperature effects during welding. Relationship among welding, microstructure and residual stress will be discussed.

Experimental process

Materials and welding process. Two rods with Ø 24 mm diameter of as-rolled AA7020-T6 Al alloy (90 mm in length) and 316L steel (100 mm in length) were used as initial materials with their chemical compositions listed in Tab. 1. The 316L steel was preheated before the friction welding for 45 minutes at 500 ± 10 ° C and then added directly to the AA7020-T6 with rotational speed of 1476 rpm, as shown in Fig. 1 describing the whole RFW process. The AA7020-T6 rod was first pressed onto the 316L steel with a compressive load of 190 MPa. The rotation of 316L steel was stopped when the length of the Al rod was shortened by 3.2 mm. The compressive load was then immediately raised to 320 MPa and kept 5 s which increased the length of friction shortened section of the Al rod to 11.5 mm.

Tab.1 Chemical compositions of AA7020-T6 and 316L steel, respectively (in wt.%).

AA7020-T6	Zn	Mg	Fe	Mn	Zr	Cu	Si	Ti	Al
	4.4	1.25	0.32	0.31	0.14	0.01	0.06	0.01	Bal.
316L	C	Mn	Si	P	S	Cr	Ni	Mo	Fe
	0.03	2.0	0.75	0.045	0.03	16	10.0	2.0	Bal.

Optical microstructure (OM) observation. The cylinder sample was cut into two halves via electrical discharge machining. The flat surface of one half-cylinder was then grinded and polished for the SEM/EDAX element analysis. Picric acid and 20% NaOH were used to etch the steel and AA7020-T6 surface separately for optical microstructure observation.

Texture measurement. Pole figure measurement on the cylinder sample was done using the robot system at the STRESS-SPEC neutron diffractometer (FRM II, Garching Germany), because other than using a conventional Eulerian cradle [9] the texture analysis along the rotation axis on both sides can be done with one setup. A monochromatic beam with wavelength of 1.69 Å from a Ge (311) monochromator was selected. The positions were the pole figure were measured are schematically shown in Fig. 2. To increase the grain statistics different gauge volumes were selected for the different positions: e.g. at A and D a volume of 5×5×5 mm^3, at position B a volume of 3×3×3 mm^3 and at position C a volume of 2×2×2 mm^3 was used.

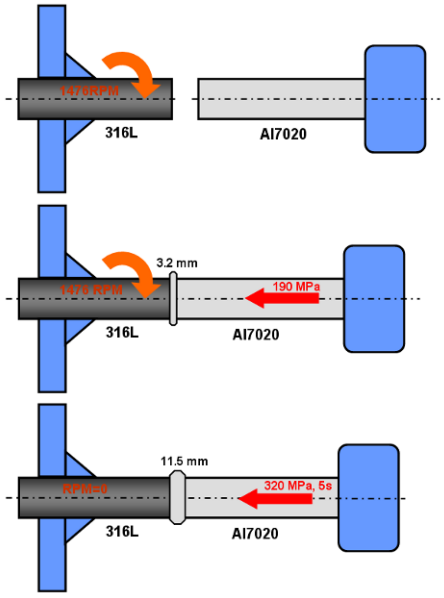

Fig. 1 Schematic illustration of the friction welding processing.

Residual stress analysis. A monochromatic beam with wavelength of 1.68 Å from Si (400) was selected for strain scanning, which allows using the desired Bragg reflections at a scattering angle of 2Θ~90°. The gauge volume was 2×2×2 mm^3 set by incoming and outgoing slits, as shown in Fig. 3. Strains (in radial, hoop and axial direction) were calculated from the fitted reflection positions of 316L- (311) and AA7020-T6 - (311) and the strain free reference value form a 1×1×1 mm^3 cube sample machined from each matrix material [11] using following relationship: $\varepsilon = (\sin\theta_0/\sin\theta)-1$.

From the strains the residual stresses were calculated using the diffraction elastic moduli and Poisson ratio of AA7020-T6 E_{Al} (311) = 69.7 GPa and ν_{Al}(311)= 0.342; and E_{Aus} (311) = 195 GPa and ν_{Aus} (311) = 0.29 for 316L austenitic steel, respectively.

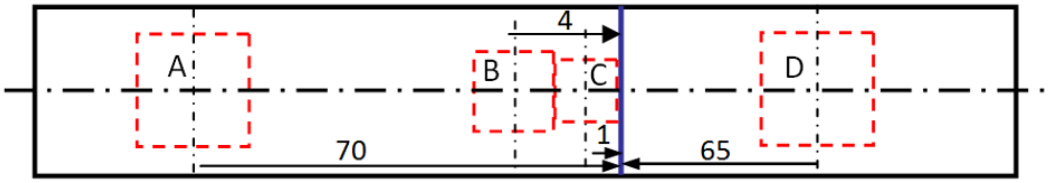

Fig. 2 Texture measurement positions A, B, C and D, respectively. For clarity the size of the gauge volumes is shown not to scale.

Results and discussion

Microstructures. Fig. 4 shows optical microstructures around the weld region. At the AA7020-T6 side shearing bands around the central rotation axis are clearly visible with recrystallized grains in between the shearing bands also observed. A zone of about 200 µm thickness free of shearing bands can be identified close to the weld line corresponding to the deformation zone under high temperature during friction welding. The 316L steel side shows no change of microstructure suggesting almost no deformation or temperature effect. Fig. 5 shows the result of an EDX scan from two different lines, 1 and 2, across the weld line. A dark layer near the white bonding boundary is clearly observed which stems from the materials flow of AA7020-T6. A high oxygen concentration was observed in this layer. No chemical variation was found at 316L steel side in both lines.

Fig. 3 Setup for the axial direction strain scanning of the welded rod.

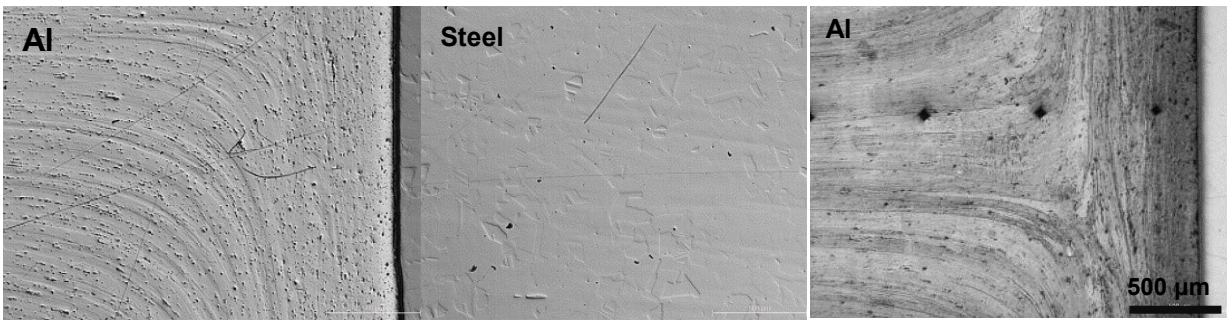

Fig. 4 OM microstructures near the weld line.

Texture evolution. Fig. 6 left shows the measured (111) and (200) pole figures at position D of the 316L steel. Both pole figures show a weak intensity distribution with a maximum of 1.4 mrd (1.0 mrd is random) in (200). Two very weak possible Cube and Goss components can be identified in the 316L steel pole figures, which can be related to the as-cast ingot material [12]. Detailed texture evolution of the 316L steel around the weld line was not further performed because, first the grains are relatively large and second the EDX and OM indicated no microstructural changes due to the friction welding process. Fig. 6 right shows the texture evolution at positions A, B and C of the Al-AA7020-T6, respectively. Two strong deformation components - Brass {110} <112> and Copper {112} <111> - exist at position A and B [13]. An additional weak recrystallized Goss {110} <100> component can also be identified. While at position B the maximum intensity of the pole figure (111) was decreased by half the intensity, the Goss component remains similar in intensity as in

position A. At position C these three components are nearly destroyed. Instead a weak rotated Cube component appears which is a typical shear component in *fcc* materials [13]. This indicates plastic deformation of the AA7020-T6 during stir welding.

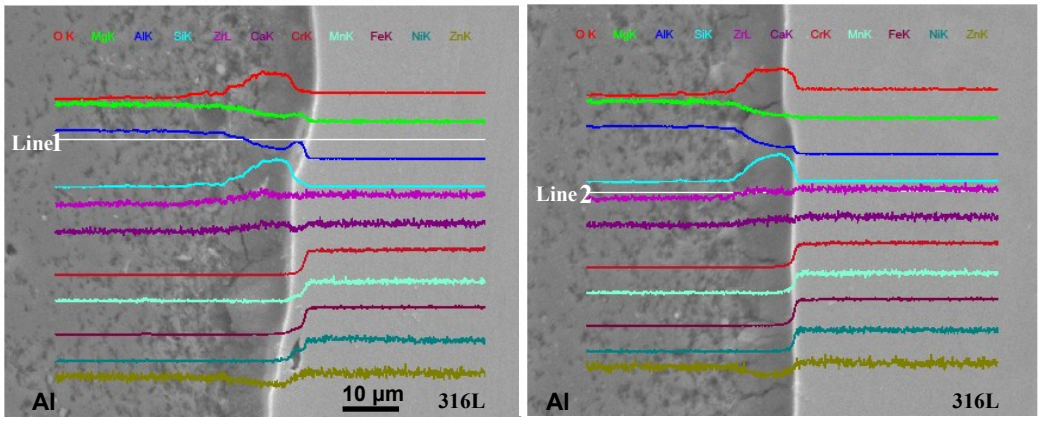

Fig. 5 EDX scan of line 1 (left) and line 2 (right) cross the weld line.

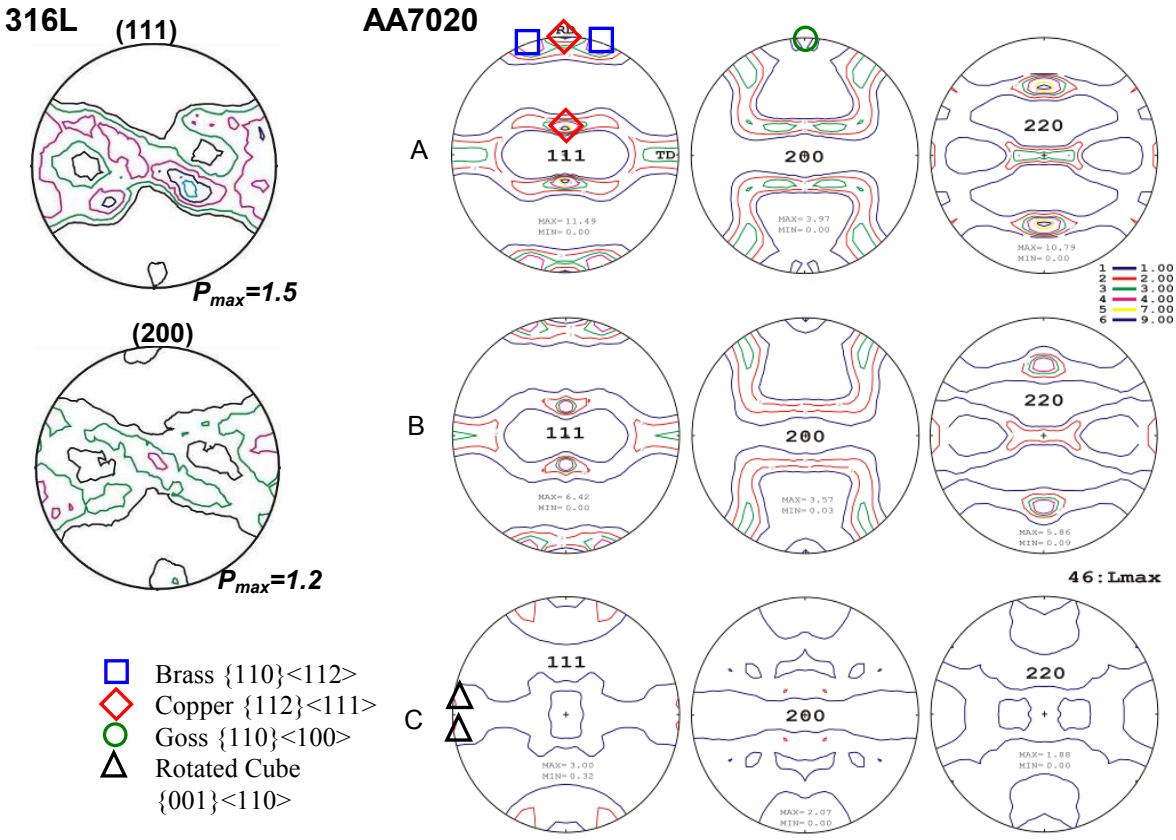

Fig. 6 Pole figures of 316L steel (left) and AA7020-T6 (right), respectively (compression direction is in the pole figure centre).

Residual stress. Fig. 7 shows the 2D residual stresses maps of half rod at a region around the weld. The black dots in the graph depict the measurement positions. Both hoop and axial residual stresses demonstrate a similar variation from the surface to the weld line. In the Al alloy tensile stresses develop from about 10 mm before the weld zone and increase to about 250 MPa at the weld line, approaching the yield strength of the material. These tensile stresses are balanced by compressive residual stress at the steel side reaching almost ~200 MPa. They gradually decrease to nearly 0 MPa at distance of 20 mm to the weld line at 316L side.

It should be mentioned that evolution of the microstructure and texture agrees well with the residual stress results. The whole welding process shows no strong influence on the microstructures of 316L steel even at the bonding interface. This is most likely due to the higher strength of this steel and a lower hot forging temperature produced during welding [2, 4]. Additional Vickers hardness measurements along the central line show a gradual increase in hardness of 316L steel from about 10 mm to the bonding interface (Fig. 8). This increase is mainly related to the high compressive residual stress.

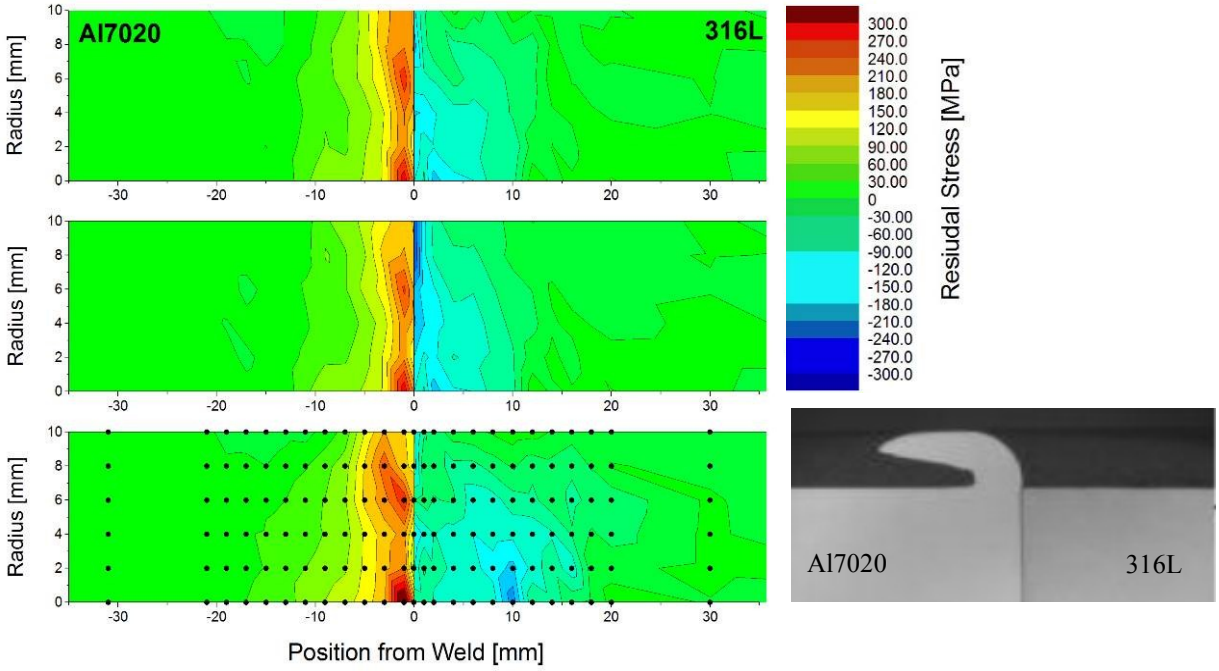

Fig. 7 Residual stress maps of the RFW weld of AA7020-T6 alloy (on the left) and 316L steel. From top to bottom are shown: radial, axial and hoop stresses.

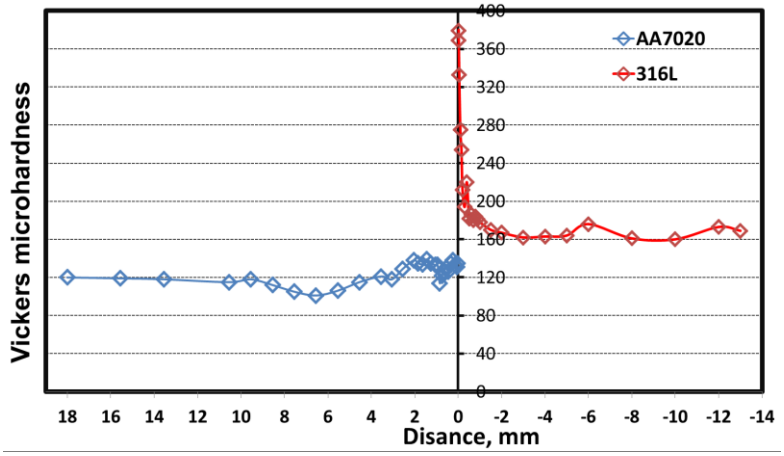

Fig. 8 Micro hardness distribution of the central line from Al (left) to steel (right).

At the side of AA7020-T6 aluminium the initial existing strong texture in the rod is reoriented around the weld line. Appearance of the shear component at region with 2 mm to the weld line is in good agreement with the observation of optical microscopy. The fast friction welding process leads to a strong plastic deformation of AA7020-T6 aluminium alloy under a combined forging and torsion stresses [2, 14]. A heat affect zone (HAZ) extending up to 10~15 mm is visible.

Moreover, a relatively high tensile residual stress (~250 MPa) in the AA7020-T6 aluminium is in-homogeneously distributed within 2 mm to the weld line. This should result from the fast plastic deformation. The maximum tensile residual stress is relatively high for aluminium alloy and could

easily initiate crack or contribute to the propagation of crack in real service [15]. Decreasing this tensile residual stress would require further optimisation of welding parameters or following heat treatments.

Summary

(1) Microstructure investigation showed a shearing band in the AA7020-T6 alloy near the weld line. No chemical and microscopic changes were observed at the 316L side of the RFW sample.
(2) Local texture analysis indicated a weak shearing component near the weld line of AA7020-T6, in good agreement with the microscopy results.
(3) Residual stress mapping by neutron diffraction demonstrated a gradual increase of a tensile residual stress with about 10 mm to the weld line at the AA7020-T6 side; and it indicated a non-uniform distribution through the diameter of the rod. A maximum compressive residual stress was obtained at the rod centre near the weld line at the 316L steel side.

References

[1] P. T. Houldcroft, Welding Process Technology, Cambridge University, Cambridge 1977.
[2] E.P. Alves, F. P. Neto, C. Y. An. J. Aerosp. Technol. Manag. 2 (2010) 301-306.
[3] N. S. Kalsi, V. S. Sharma, Int. J. Adv. Manuf. Technol. 57 (2011) 957-967.
[4] Y.L. Song, Y.G. Liu, X.Y. Zhu, S.R. Yu, Y.B. Zhang, Trans. Nonferrous Met. Soc. China 18 (2008) 14-18.
[5] M. Avinash, G. V.K. Chaitanya, D.K. Giri, S. Upadhya, B.K. Muralidhara, World Acad. of Sci. Eng. & Tech. 11 (2007) 146-148.
[6] V. Ventzke, H.-G. Brokmeier, P. Merhof, M. Koçak, Solid State Phenon. 160 (2010) 319-326.
[7] P.D. Sketchley, P.L. Threadgill, I.G. Wright, Mater. Sci. & Eng. A329-331 (2002) 756-762.
[8] R.S. Mishra, Z.Y. Ma, Mater. Sci. & Eng. R50 (2005) 1-78.
[9] H.-G. Brokmeier, W.M. Gan , C. Randau, M. Voeller, J. Rebelo-Kornmeier, M. Hofmann, Nucl. Instr. & Meth. in Phy. Res. A642 (2011) 87-92.
[10] M. Hofmann, W. M. Gan, J. Rebelo-Kornmeier, M. Schoebel, Neutron News (2013) 14-17.
[11] A.J. Allen, M.T. Hutchings, C.G. Windsor, C. Andreani, Adv. in Phys. 34 (1985) 445-473.
[12] H. Hu, Texture, 1 (1974), 233- 258.
[13] H.R. Wenk, P.V. Houtte, Rep. Prog. Phys. 67 (2004) 1367-1428.
[14] M. Perovic, D. Veljic, M. Rakin, N. Radovic, A. Sedmak, N. Bajic, Mater. & Techno. 46 (2012) 215-221.
[15] K. Mumar, S. V. Kailas, Mater. & Design, 29 (2008) 791-797.